

A015

Salt Flank Exploration - 3D CSEM Imaging in the SEAM Model

J.P. Morten* (EMGS) & K. Kumar (EMGS)

SUMMARY

We have simulated a salt flank hydrocarbon reservoir imaging case using the 3D controlled source electromagnetic data from the SEAM phase I model. The complication due to the dominant EM response from the salt body is tackled by a structural constraint. In our simulated exploration scenario, we assumed that seismic imaging provided information to construct an approximate salt structural model but with three types of errors: 1) Limited information below salt overhangs and no base salt, 2) inaccurate lateral and depth positioning, and 3) incorrect salt resistivity. A modeling study and our imaging results demonstrate that the applied workflow is robust against these errors, and the 3D inversion results in a reconstruction that agrees well with the true model reservoir laterally and in depth.

Introduction

Traps for hydrocarbon reservoirs can be formed at the flanks of salt bodies, and therefore salt flanks are highly interesting for hydrocarbon exploration. However, imaging and interpretation of salt flank targets can be difficult due to the presence of the salt, which significantly affects both seismic and controlled source electromagnetic (CSEM) data. Reservoir fluid discrimination using CSEM utilizes the fact that a hydrocarbon saturated reservoir represents a resistive anomaly. However, a salt body will also be highly resistive and can give a data response that exceeds in magnitude the response which is caused by the hydrocarbon reservoir. The CSEM imaging challenge is therefore to differentiate the hydrocarbon reservoir and salt response in the data.

We have conducted a synthetic case study on the phase I model of the SEG Advanced Modeling Corporation (SEAM). This model is representative for deepwater regions in the Gulf of Mexico, and contains a large salt structure and several reservoirs. Figure 1a shows a 3D view of the salt body with two of the hydrocarbon reservoirs. In this study, we focus on the highlighted upper reservoir which is located partly below a salt overhang. For this model, we aim to solve the CSEM imaging challenge described above by incorporating the partial information about the salt body structure shown in Figure 1b. This structural information is assumed to be available from the results of a seismic survey. In this paper, we will first describe how we created the background resistivity model, and then present our 3D inversion which gives good imaging of the hydrocarbon reservoir at the salt flank.

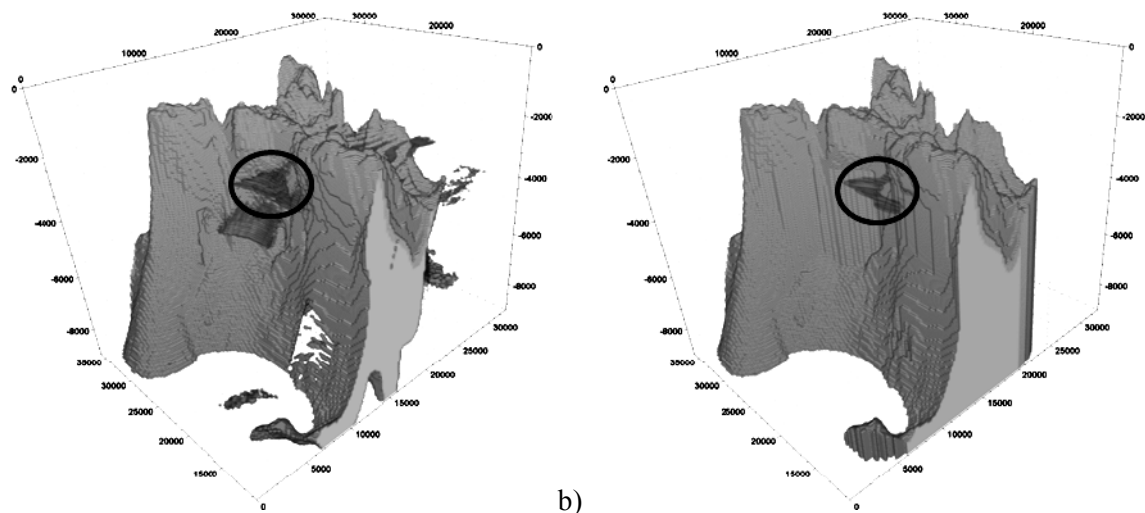


Figure 1 3D view of the salt body in the SEAM phase I model for a) the true model, and b) the inversion final model from the hydrocarbon reservoir imaging study. The target hydrocarbon reservoir has been highlighted by an ellipse.

SEAM salt model

Geophysical imaging is challenging in the deepwater Gulf of Mexico because hydrocarbon reservoirs are often obscured by massive, complex salt bodies. The SEAM initiative aims to advance geophysical imaging in this region by providing the industry and the geophysical research community with a realistic benchmark geological model, along with synthetic geophysical datasets (Stefani et al., 2010; Fehler, 2011). The SEAM model seismic data has been utilized already in several applications of salt imaging and inversion (see e.g. Bulcão et al., 2011 for a recent example).

The SEAM resistivity model has VTI anisotropy in the background, while the salt body is isotropic and homogeneous with resistivity 100 Ωm . The thickness of the salt is up to 5 km. The background resistivity varies with depth from approximately 0.5 to 4 Ωm , and the ratio of the vertical to the horizontal resistivity varies approximately in the range 0.5 to 3. The water is isotropic with resistivity 0.3 Ωm , and the water depth varies in the range 1-2 km. In this study, we consider imaging of the turbidite fan reservoir of Pleistocene age highlighted in Figure 1a. The burial depth is 1-1.5 km below

the seafloor, and the resistivity is about 40 Ω m. This resistivity would correspond to a hydrocarbon saturation of 80 % for typical parameters of the Archie rock physics model for sandstones. The typical thickness of the reservoir is 40 m, and laterally its area is approximately 30 km². Another reservoir located at a deeper level (burial depth 2.1-3.1 km) overlaps laterally with our target, but CSEM modeling indicates that the sensitivity towards the deeper reservoir will be very limited. The target reservoir is located at the salt flank, terminating directly onto the salt. The salt flank in the reservoir area has some overhang above the reservoir, i.e. the salt withdraws laterally with increasing depth. At the south end of the target reservoir, the overhang covers a 500 m wide zone over the reservoir, with further salt withdrawal below that level.

CSEM is an inherently low-frequency method, with associated limited spatial resolution. Seismic imaging can incorporate high frequencies and give more detailed structural models for e.g. a top salt surface. Salt imaging using the SEAM seismic data has been considered by several authors, for example Bulcão et al. (2011). We will assume that some structural information from seismic imaging is available to constrain the geometry of the salt body, but introduce two types of errors in the structural model to simulate the complications of base salt imaging. First, base salt structure is only included to define overhangs down to approximately 1.5 km below seafloor at the salt flanks. Below this level, our input salt body structural model represents a flooded model, i.e. the salt body is defined only from a top salt horizon and is unbounded below. The difference between the true salt geometry and our input salt body can be seen in Figure 1. Second, we assume that e.g. the velocity model was not known accurately, and introduce a spatial translation of the salt body. The discrepancy between the position of the true salt body and the top salt horizon in our structural model is 240 m in both lateral directions, and 80 m vertically.

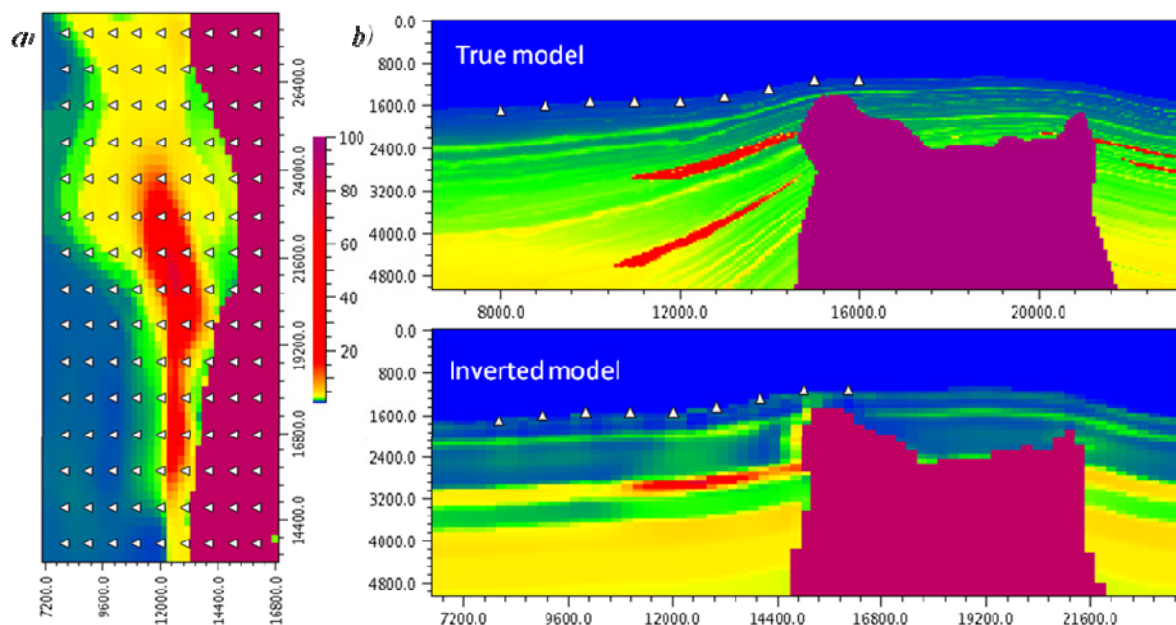


Figure 2 3D inversion result comparison with receiver locations (white triangles). a) Horizontal slice from inverted model at 2850 m. b) Vertical section along the central east-west receiver line, for the true model (top) and the inverted model (bottom). The position and extent of the red high-resistivity region in the inverted model corresponds well with the true model hydrocarbon reservoir target.

CSEM input data and the imaging challenge

To reliably image the hydrocarbon reservoir at the salt flank, the ambiguity of the response due to the reservoir and the nearby salt must be resolved. The presence of the salt body can give an order of magnitude increase in electric field amplitude, whereas the introduction of the hydrocarbon reservoir studied here gives an amplitude increase of typically 40 %. This large difference in the magnitude of the responses means that unless the response due to salt can be constrained as part of the background,

we cannot expect an accurate imaging result from the much smaller response due to the hydrocarbon reservoir where the responses overlap in space. The reservoir terminates at the salt flank under an overhang, but the majority of the reservoir is laterally separated from the salt body. The lateral resolution of the CSEM data is related to the wavelength of the highest frequency data component with significant sensitivity at target depth, as well as receiver density. The spatial overlap of the salt and reservoir responses is on a similar scale and we expect that by constraining the extent of the salt body laterally, the response due to the reservoir can be identified and imaged in inversion.

The CSEM survey layout is shown in Figure 2a, and comprises 135 receivers in a 1 km × 1 km grid. Data from 9 North-South towlines and 15 East-West towlines are included. The inversion input amplitude and phase data was contaminated with Gaussian noise where the standard deviation was chosen at 3 % of the data amplitude. We use the electric field data, and include only records with amplitude above 10^{-15} V/m to ensure that the dataset is representative of that which could be acquired in a real case. The CSEM data will be processed by the 3D inversion described by Zach et al. (2008). To obtain good convergence properties, we constructed an initial 3D model that approximately describes the overall background trends. To determine an approximate resistivity profile for the overburden, we performed 1D simulated annealing inversion (Roth and Zach, 2007). The receiver and source locations included for the 1D inversion are located off the salt body, thus the 1D assumption will be valid where the bedding is approximately flat. We then created a 3D background model consistent with the true bathymetry based on the 1D profile. This was done by identifying the depth in the 1D profile with burial depth. The seafloor is uplifted over the salt, which introduces a tilt to the layers found by 1D inversion close to the salt body.

The salt body will be defined by the approximate structural model described above. The true model salt body is homogeneous and isotropic with resistivity 100 Ωm . We do not assume that the salt resistivity is known a priori, but assume that a homogeneous and isotropic description suffices. At frequency 1.0 Hz, the skin depth in a medium of 100 Ωm is 5 km, and thus the isotropy assumption is valid when any intrinsic, predominant orientation averages out over this length. Furthermore, if the average resistivity over the same length scale varies slowly, the assumption of homogeneity will be valid for a large volume of the salt close to the flank.

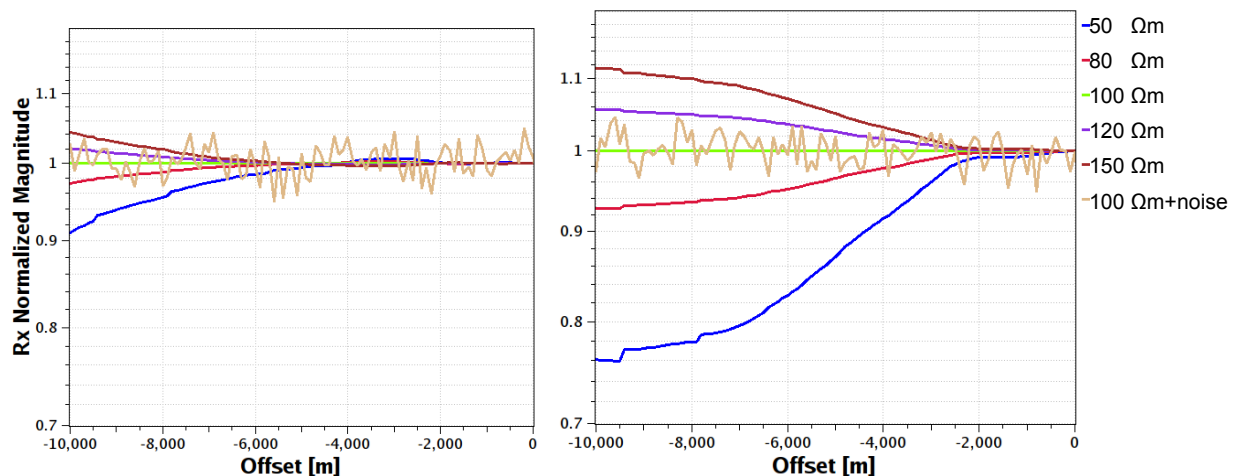


Figure 3 Electric field amplitude for inline (left) and broadside (right) data at 0.4 Hz for a model with variable salt resistivity, normalized to the data from the true model. The noisy curve is representative of the actual input data which was contaminated with noise.

We performed a sensitivity study to determine the importance of an accurate salt resistivity value, considering modelled CSEM data for an inline and a broadside source towed along the north-south towline farthest east. A deep-towed broadside source is not currently available for real data acquisition, and in the inversion input data, it will be the azimuth data from receivers off the active towline that contribute broadside measurements. The inline normalized responses shown in Figure 3 are typically on the scale of the random variations in the input data where we added noise, so inline

data have low sensitivity to the actual salt resistivity when varied in the range 80 to 120 Ωm . Broadside data have larger sensitivity to the actual salt resistivity, but variation in the range 90-110 Ωm seems not to be resolved well. We see this non-uniqueness as a strength of the suggested methodology, since imaging of the hydrocarbon reservoir is likely to be robust against small errors in salt resistivity. To simulate the effect of imperfect information in inversion, we use a constant salt resistivity that is 10 Ωm smaller than the true model resistivity.

3D Inversion

We carried out 3D CSEM inversion, and constrained the salt body according to the imperfect structure and resistivity model described above. The horizontal electric field records at frequencies 0.2, 0.4, and 0.8 Hz for all towlines was included at each receiver. As mentioned above, the input data had been contaminated by 3 % Gaussian noise, and samples with amplitude lower than 10^{-15} V/m were omitted. Figure 2 shows that the reservoir has been imaged clearly, and the recovered depth and lateral extent corresponds well with the true model. The discrepancy between the input data and the inverted model synthetic data is on the level of the data uncertainty given the added noise.

Conclusions

A challenge for CSEM imaging of salt flank hydrocarbon reservoirs is that the salt body EM response can be an order of magnitude larger than the response due to the reservoir, and that these responses can overlap in space. We have studied this problem in context of the SEAM phase I salt model, and utilize structural information about the salt body in conjunction with CSEM data. The structural information could be the result of top salt mapping from wide azimuth seismic data, but we assume that this structure will not be known accurately. To be realistic, our imaging study therefore incorporates significant discrepancies between the input information about the salt body structure and resistivity compared to the true model. Our study demonstrates how the input structural information can be used to resolve the ambiguity between the salt and reservoir responses, and give good imaging results. We believe our encouraging results can be relevant for the planning of integrated CSEM and seismic exploration surveys in areas where prospects are located in the vicinity of background resistive structures related to e.g. salt bodies, basement, basalt, or carbonate.

Acknowledgements

We would like to acknowledge SEG Advanced Modeling Corporation (SEAM) for their initiative to create the realistic salt model used for this study. We are also thankful to RPSEA (Research Partnership to Secure Energy for America) for funding the CSEM simulations to SEAM under the Ultra-Deepwater Program. We are also thankful to EMGS for permission to publish this paper.

References

- Bulcão, A., Soares Filho, D.M., Catão Alves, G., do Vale Moreira, T., van den Berg, P. and Gisolf, D. [2011] Improved RTM depth image with full waveform inversion. *SEG Expanded Abstracts*, **30**, 2783 (2011).
- Fehler, M. [2011] SEAM update: Phase I-RPSEA progress includes new activities. *The Leading Edge* **30**, 982 (2011).
- Roth, F. and Zach, J.J. [2007] Inversion of marine CSEM data using up-down wavefield separation and simulated annealing. *SEG Expanded Abstracts*, **26**, 524 (2007).
- Stefani, J., Frenkel, M., Bundalo, N., Day, R. and Fehler, M. [2010] SEAM update: Models for EM and gravity simulations. *The Leading Edge*, **29**, 132 (2010).
- Zach, J.J., Bjørke, A.K., Støren, T. and Maaø, F. [2008] 3D inversion of marine CSEM data using a fast finite-difference time-domain forward code and approximate hessian-based optimization. *SEG Expanded Abstracts*, **27**, 614 (2008).